JACS
JOURNAL OF THE AMERICAN CHEMICAL SOCIETY
Article
Cite This: J. Am. Chem. Soc. 2018, 140, 3040−3051
pubs.acs.org/JACS

Control of Electronic Structure and Conductivity in Two-Dimensional Metal−Semiquinoid Frameworks of Titanium, Vanadium, and Chromium

Michael E. Ziebel,[†] Lucy E. Darago,[†] and Jeffrey R. Long*[,†,‡,§]

[†]Department of Chemistry, University of California, Berkeley, California 94720, United States
[‡]Department of Chemical and Biomolecular Engineering, University of California, Berkeley, California 94720, United States
[§]Materials Sciences Division, Lawrence Berkeley National Laboratory, Berkeley, California 94720, United States

Supporting Information

ABSTRACT: The isostructural, two-dimensional metal−organic frameworks $(H_2NMe_2)_2M_2(Cl_2dhbq)_3$ (M = Ti, V; Cl_2dhbq^{n-} = deprotonated 2,5-dichloro-3,6-dihydroxybenzoquinone) and $(H_2NMe_2)_{1.5}Cr_2(dhbq)_3$ ($dhbq^{n-}$ = deprotonated 2,5-dihydroxybenzoquinone) are synthesized and investigated by spectroscopic, magnetic, and electrochemical methods. The three frameworks exhibit substantial differences in their electronic structures, and the bulk electronic conductivities of these phases correlate with the extent of delocalization observed via UV−vis−NIR and IR spectroscopies. Notably, substantial metal−ligand covalency in the vanadium phase results in the quenching of ligand-based spins, the observation of simultaneous metal- and ligand-based redox processes, and a high electronic conductivity of 0.45 S/cm. A molecular orbital analysis of these materials and a previously reported iron congener suggests that the differences in conductivity can be explained by correlating the metal−ligand energy alignment with the energy of intervalence charge-transfer transitions, which should determine the barrier to charge hopping in the mixed-valence frameworks.

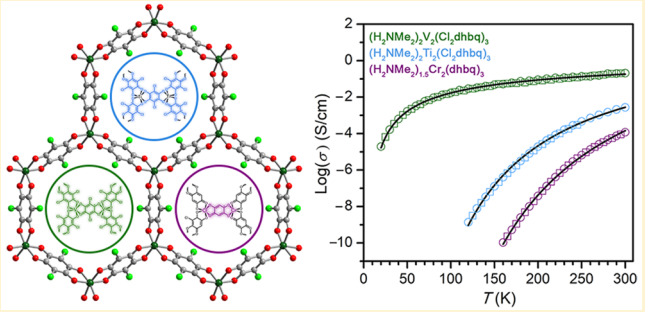

INTRODUCTION

Long-range electron correlation giving rise to electronic conductivity in solid-state materials is typically dependent on short metal−metal distances and diffuse covalent interactions that can facilitate orbital interactions between neighboring metal centers. In contrast, the chemistry of metal−organic frameworks largely relies on the use of ionic metal−ligand interactions and large distances between metal nodes to generate rigid, porous structures.[1] While these properties make such framework materials promising for applications in gas storage, gas separations, and catalysis, their potential in electronic applications has been limited by the insulating character that arises from these ionic interactions.[2] Indeed, most metal−organic frameworks display highly localized electronic structures with little charge dispersion.[3] However, if long-range electronic interactions could be achieved in these materials, the concomitant ability to tune their surface chemistry and electronic structure via modification of metal, ligand, and network topology could prove to be a powerful means of customizing their functionality within electronic devices.[4]

A growing number of metal−organic frameworks and related coordination solids have been shown to display electronic conductivity.[5] These reports have demonstrated a variety of structural motifs that promote long-range electron delocalization, including metal−thiolate chains, infinite $\pi-\pi$ stacks, donor−acceptor charge-transfer chains, and $\pi-d$ conjugated square planar metal sites.[6] Furthermore, frameworks containing mixed-valence units that repeat in one-, two-, or three-dimensions have been shown to display significantly improved electronic conductivities compared to their valence-pure counterparts.[7]

Despite increased interest in the electronic properties of metal−organic materials, there are few systematic studies investigating the effects of metal ion substitution on electronic structure across a series of isostructural frameworks. In fact, few metal−organic frameworks display semiconducting character across multiple metals, making it challenging to develop design principles for new conductive materials.[8] A series of tetrathiafulvalene (TTF) based frameworks $M_2(TTFTB)$ (M = Mn, Co, Zn, Cd; $TTFTB^{4-}$ = tetrathiafulvalene-tetrabenzoate) was shown to display metal-dependent conductivity, but the conduction pathway of these materials does not directly involve the metal centers; rather, differences in conductivity were assigned to differences in the TTF $\pi-\pi$ stacking distance.[9] Similarly, a series of TCNQ-based materials $M(TCNQ)_2$ (M = Mn, Fe, Co, Ni, Cu; TCNQ = tetracyanoquinodimethane) was

Received: December 21, 2017
Published: February 5, 2018

DOI: 10.1021/jacs.7b13510
J. Am. Chem. Soc. 2018, 140, 3040−3051

found to display changes in conductivity with metal substitution, but these differences have not been explained with a cohesive model.[10]

The principles of molecular coordination chemistry should be well-suited for application in the design of framework structures that display high electronic conductivity. The degree of delocalization in compounds containing redox non-innocent ligands has been thoroughly explored via spectroscopic, magnetic, and computational methods, resulting in molecular orbital models that can readily explain the observed properties.[11] Furthermore, delocalization in mixed-valence molecules has been described using a molecular orbital approach.[12] Despite the classification of metal−organic frameworks as molecule-based materials, orbital models have seldom been used to explain their bulk electronic properties.

Frameworks incorporating 2,5-dihydroxybenzoquinone (H_2dhbq) and its analogues as a linker are particularly well suited for an orbital-based analysis. This ligand system has been shown to bind to metal ions in three different redox states in both molecular complexes and extended solids (Figure 1).[13]

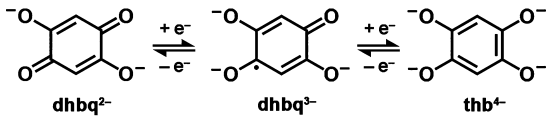

Figure 1. Redox states of the linker 2,5-dihyroxybenzoquinone that have been observed in metal−organic complexes and materials.

The low-lying π^* orbitals of H_2dhbq are close in energy to the d orbitals of the transition metals, facilitating metal−ligand electron transfer and long-range orbital interactions between metal centers.[14] Importantly, molecular orbital models developed for tris-catecholate complexes should translate well to the octahedral building units of frameworks generated from this ligand (Figure 2).[15]

Two- and three-dimensional materials of the general formula $(\text{cation})_2M_2(X_2\text{dhbq})_3$ have been synthesized with all of the late first-row transition metals (M = Mn, Fe, Co, Ni, Cu, and Zn; X = a proton or halide).[13d,16] While most of these materials are insulating and exhibit weak magnetic interactions, the two- and three-dimensional iron phases were observed to display high electronic conductivities and strong magnetic coupling.[13d,17] These properties were attributed to ligand mixed-valency, arising from reduction of a portion of the dhbq^{2-} molecules to dhbq^{3-} by the iron(II) reactants, yielding frameworks containing iron(III) centers bridged by a mixed-valence ligand scaffold: $[Fe^{III}_2(X_2\text{dhbq}^{2-})(X_2\text{dhbq}^{3-})_2]^{2-}$.

Expanding on this prior work, we herein report the synthesis and electronic properties of the two-dimensional titanium, vanadium, and chromium analogues of the iron framework. The electronic structures of these frameworks are examined via spectroscopic and magnetic susceptibility measurements, revealing large differences in the extent of electron delocalization. The conductivities of the materials are moreover shown to correlate with their electronic structures, with the vanadium phase displaying the highest conductivity as a result of substantial metal−ligand covalency.

EXPERIMENTAL SECTION

General Information. All syntheses and manipulations were performed in an Ar-atmosphere MBraun glovebox, with the exception of the synthesis and purification of the chromium framework. The solvents *N*,*N*-dimethylformamide (DMF) and tetrahydrofuran (THF) were dried using a commercial solvent purification system designed by JC Meyer Solvent Systems and were stored over 4 Å molecular sieves prior to use. All other compounds were purchased and used as received. The compounds $Cr(NO_3)_3{\cdot}9H_2O$ (99%), 2,5-dihydroxybenzoquinone (98%), and titanium(II) chloride (99%) were purchased from Sigma-Aldrich, vanadium(II) chloride (99.9%) was purchased from American Elements, 2,5-dichloro-3,6-dihydroxybenzoquinone (98%) was purchased from Alfa Aesar, and sodium hydroxide (99%) was purchased from Fisher Scientific. Carbon, hydrogen, and nitrogen analyses were obtained from the Microanalytical Laboratory at the University of California, Berkeley.

Synthesis of $(H_2NMe_2)_2Ti_2(Cl_2\text{dhbq})_3{\cdot}4.7$DMF (1-Ti). In an Ar-filled glovebox, $TiCl_2$ (10 mg, 0.084 mmol) and 2,5-dichloro-3,6-dihydroxybenzoquinone (34 mg, 0.16 mmol) were combined in 10 mL of DMF in a 20 mL borosilicate vial. The suspension was heated to 120 °C for 24 h, and then allowed to cool to room temperature. The resulting black powder was filtered, washed with 10 mL of DMF, and suspended in 10 mL of fresh DMF. This was repeated two more times until the filtrate was colorless. The remaining microcrystalline black solid was dried at room temperature under reduced pressure for 1 h to afford the product. Yield: 10 mg (21%). Anal. Calcd for $C_{36.1}Cl_6H_{48.9}N_{6.7}O_{16.7}Ti_2$: C, 37.6; H, 4.3; N, 8.1. Found: C, 37.2; H,

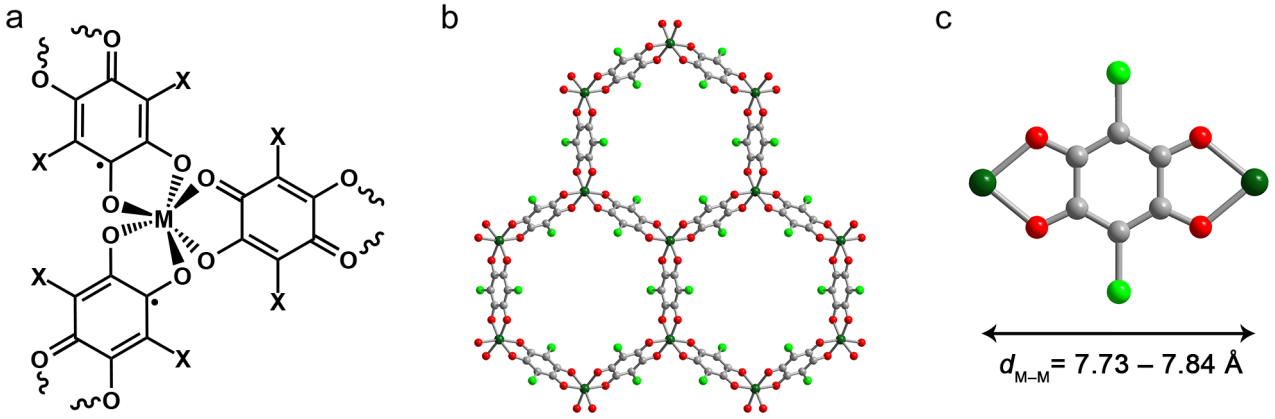

Figure 2. (a) Illustration of the octahedral building unit found in both the two- and three-dimensional frameworks of 2,5-dihydroxybenzoquinone. Two of the ligands are shown as dhbq^{3-}, as was observed for the previously reported iron phases. (b) Structure of a single sheet from the two-dimensional phase viewed down the one-dimensional pore (*c*-axis). Metal, C, O, and Cl atoms are shown as dark green, gray, red, and light green spheres, respectively. Solvent molecules and dimethylammonium cations contained within the pore are removed for clarity. (c) Representative dimetallic unit in the two-dimensional phase; the shortest metal−metal distances in **1-Ti**, **2-V**, and **3-Cr** are 7.84, 7.79, and 7.73 Å, respectively.

DOI: 10.1021/jacs.7b13510
J. Am. Chem. Soc. 2018, 140, 3040−3051

4.7; N, 8.5. IR (solid-ATR): 3069 (w), 2922 (w), 2853 (w), 2797 (w), 2762 (w), 2478 (w), 2439 (w), 1651 (vs), 1554 (w), 1404 (vs) 1353 (vs), 1277 (m), 1245 (s), 1192 (m), 1090 (m), 1045 (m), 1002 (vs), 966 (s), 897 (w), 839 (s), 748 (w), 661 (m), 609 (w), 581 (w), 504 (vs).

Synthesis of $(H_2NMe_2)_2V_2(Cl_2dhbq)_3$·6.4DMF (2-V). In an Ar-filled glovebox, VCl_2 (20 mg, 0.16 mmol) and 2,5-dichloro-3,6-dihydroxybenzoquinone (34 mg, 0.16 mmol) were combined in 10 mL of DMF in a 20 mL borosilicate vial. The suspension was heated to 120 °C for 30 h, and then allowed to cool to room temperature. The resulting black powder was filtered, washed with 10 mL of DMF, and suspended in 10 mL of fresh DMF. This washing procedure was repeated two more times until the filtrate was colorless. The remaining microcrystalline black solid was dried at room temperature under reduced pressure for 1 h to afford the product. Yield: 6 mg (9%). Anal. Calcd for $C_{41.2}Cl_6H_{60.8}N_{8.4}O_{18.4}V_2$: C, 38.5; H, 4.8; N, 9.2. Found: C, 38.6; H, 5.0; N, 9.2. IR (solid-ATR) 1643 (w), 1471 (w), 1221 (w), 965 (w).

Synthesis of $(H_2NMe_2)_{1.5}Cr_2(dhbq)_3$·4.4DMF (3-Cr). In air, a thick-walled borosilicate tube was charged with 140 μL of 1 M $Cr(NO_3)_3$ in distilled water, 2,5-dihydroxybenzoquinone (40 mg, 0.28 mmol), 40 μL of 0.2 M aqueous sodium hydroxide, and 1.4 mL of anhydrous DMF. The reaction mixture was degassed via three freeze–pump–thaw cycles, after which the tube was flame-sealed and placed in an oven preheated to 120 °C. After heating for 18 h, the tube was removed from the oven and allowed to cool to ambient temperature. The resulting purple powder was then filtered inside a Vacuum Atmospheres glovebox with a humid nitrogen atmosphere. The powder was suspended in 10 mL of DMF for 24 h and was then recollected by filtration. This washing procedure was repeated two more times until the filtrate was colorless. The remaining microcrystalline solid was washed with 1 mL of THF and then dried at room temperature under reduced pressure for 20 min to afford the product. Yield: 55 mg (87%). Anal. Calcd for $C_{33.9}Cr_2H_{48.1}N_{5.8}O_{16.3}$: C, 45.1; H, 5.4; N, 9.0. Found: C, 45.3; H, 5.1; N, 9.4. IR (solid-ATR): 3051 (w), 2931 (w), 2849 (w), 2801 (w), 2478 (w), 1665 (vs), 1540 (s), 1450 (vs), 1372 (s), 1295 (w), 1195 (vs), 1090 (m), 1024 (w), 872 (m), 819 (w), 758 (w), 661 (m), 568 (s), 509 (s).

RESULTS AND DISCUSSION

Syntheses and Structures. Among the reported dhbq-based frameworks containing late transition metals, only the iron phases display a metal-to-ligand electron transfer that yields a mixed-valence framework.[18] This observation suggested that highly reducing divalent transition metals would be required to generate isostructural frameworks with similar electronic structures, and so we turned to the early transition metals—titanium, vanadium, and chromium—in an attempt to access congeners with improved electronic properties. In addition to the highly reducing nature of Ti^{2+}, V^{2+}, and Cr^{2+}, these early transition metals have higher-energy and more diffuse 3d orbitals than iron, which we expected would improve energy alignment and orbital overlap with the π^* orbitals of the ligand, leading to stronger magnetic coupling and increased electrical conductivities. Octahedral tris-catecholate complexes resembling the metal nodes within these frameworks have also been reported for all three early transition metals, and thus we were encouraged that the intended phases could be obtained.[18]

Initial efforts to synthesize the two-dimensional semiquinoid frameworks of titanium, vanadium, and chromium began with the reaction of the divalent metal salts with H_2dhbq or chloranilic acid (H_2Cl_2dhbq) in DMF, conditions similar to those reported for the two-dimensional iron phase.[13d] The reaction of 0.5 equiv of titanium(II) chloride or 1 equiv of vanadium(II) chloride with H_2Cl_2dhbq in anhydrous DMF yielded black crystalline powders identified as $(H_2NMe_2)_2Ti_2(Cl_2dhbq)_3$·4.7DMF (**1-Ti**) and $(H_2NMe_2)_2V_2(Cl_2dhbq)_3$·6.3DMF (**2-V**). Analogous reactions using H_2dhbq yielded only poorly crystalline products. Compounds **1-Ti** and **2-V** represent the first crystalline extended solids featuring $dhbq^{n-}$-type ligands with titanium and vanadium.[19]

Analogous synthetic procedures using $CrCl_2$ and other chromium(II) sources failed to yield crystalline products; as such, alternative synthetic strategies were pursued. Recently, an isostructural aluminum framework was reported, wherein ligand-based mixed-valence was thought to result from partial ligand reduction by dimethylammonium formate, formed upon hydrolysis of DMF, rather than from metal-to-ligand electron transfer.[20] Using similar reaction conditions with $Cr(NO_3)_3$ and H_2dhbq afforded a crystalline purple powder determined to be $(H_2NMe_2)_{1.5}Cr_2(dhbq)_3$·4.3DMF (**3-Cr**). Attempts to synthesize this phase with H_2Cl_2dhbq did not yield the desired product. While some differences in electronic properties can be expected for frameworks incorporating $dhbq^{n-}$ in place of Cl_2dhbq^{n-}, the effects of metal substitution are expected to play a much larger role than ligand modification on the overall electronic structure in these systems.[16d,21]

The powder X-ray diffraction patterns of **1-Ti**, **2-V**, and **3-Cr** confirmed that all three materials are isostructural to the reported iron phase, $(H_2NMe_2)_2Fe_2(Cl_2dhbq)_3$·6DMF·2$H_2O$ (Figure 3). The materials crystallize in the space group $P\bar{3}1m$, with unit cell parameters that increase with the ionic radius of the metal (**1-Ti** > **2-V** > **3-Cr**). The structure consists of eclipsed hexagonal honeycomb sheets with one-dimensional pores running along the *c*-axis (Figure 2b). Each metal center possesses a local D_3 symmetry and is coordinated by six O atoms from three chelating ligands, with neighboring metal centers having opposing chirality. In the three compounds, the shortest intralayer metal–metal distance is between 7.73 and 7.84 Å (Figure 2c), while the shortest interlayer metal–metal distance is between 8.65 and 8.96 Å. Due to the presence of substantial solvent and $(H_2NMe_2)^+$ ion disorder in all three structures, complete structural refinement of the powder X-ray diffraction data was not possible. Attempts to generate single-crystal products proved unsuccessful.

In the case of **1-Ti** and **2-V**, synchrotron diffraction data also revealed very small amounts of unidentified crystalline

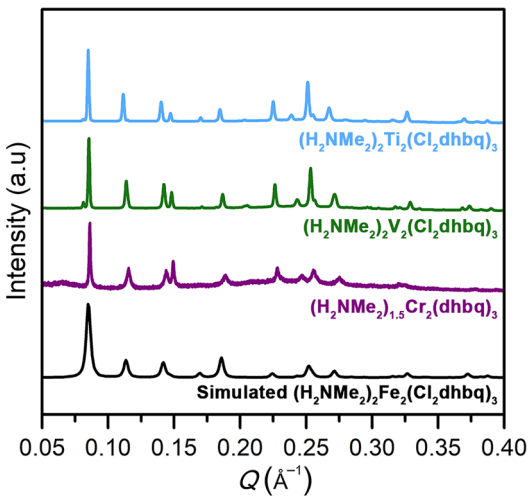

Figure 3. High-resolution powder X-ray diffraction patterns of **1-Ti**, **2-V**, and **3-Cr** compared to simulated data for the previously reported iron phase.[13d]

DOI: 10.1021/jacs.7b13510
J. Am. Chem. Soc. 2018, 140, 3040–3051

impurities. Because the only reagents used in the synthesis of these compounds were the respective metal chloride and H_2Cl_2dhbq, it seems likely that these impurities correspond to a structurally similar metal-dhbq phase, perhaps one in which a solvated metal cation replaces the dimethylammonium ions. Indeed, cation substitution has been shown to alter the symmetry of similar frameworks.[16d] Given that these impurities were present in only miniscule amounts and could not be detected on our laboratory diffractometer or by elemental analysis, it is unlikely that they affect the analysis of the electronic structure and bulk properties of the compounds.

The two-dimensional iron phase was previously reported to undergo a reversible phase transition upon activation, and to have a Brunauer–Emmett–Teller surface area of 1180 m^2/g. However, all attempts to activate **1-Ti**, **2-V**, and **3-Cr** resulted in an irreversible loss of crystallinity. Consequently, all data discussed herein were collected on solvated samples in which DMF molecules and charge-balancing dimethylammonium cations fill the one-dimensional pores.

Infrared Spectroscopy. The black color of **1-Ti** and **2-V** suggested that a metal-to-ligand electron transfer had occurred, as frameworks of $dhbq^{2-}$ and its analogues are typically red or brown.[16c,d] Similarly, reduction of the ligand during the synthesis of **3-Cr** was suggested by the change in color of the supernatant from purple to green over the course of the reaction. Infrared spectroscopy provided a means for confirming the presence of reduced ligands in each of these frameworks, as the frequency of the carbonyl stretching mode ($\nu_{C=O}$) is characteristic of the redox state of the $dhbq^{n-}$ ligand. Molecular complexes and related materials containing the dianionic ligand typically display a $\nu_{C=O}$ ranging from 1540 to 1480 cm^{-1}, while complexes containing the ligand in its trianionic state typically display a lower $\nu_{C=O}$, between 1460 and 1430 cm^{-1}.[13a,22]

The extent of delocalization in materials displaying ligand-based mixed-valence can also be probed by infrared spectroscopy. In the reported two- and three-dimensional iron phases, for example, a single IR or Raman feature was observed at a frequency between what would be expected for $dhbq^{2-}$ or $dhbq^{3-}$, suggesting electron delocalization across all three ligands on the vibrational time scale.[13d,17a] In contrast, for the aluminum congener, two distinct bands were observed in the infrared spectrum, corresponding to ligands in different redox states.[20] The lack of evidence for delocalized mixed-valence in the aluminum material is consistent with the poor energy alignment between the 3p orbitals of aluminum(III) and the π^* orbitals of the ligands, which should limit charge transfer between ligands.

Similar to iron(III), chromium(III) has half-filled π-symmetry orbitals—the t_{2g} set in an octahedral geometry—and is not sufficiently reducing to transfer additional electrons to the ligand. Thus, we expected **3-Cr** to have an electronic structure similar to the iron phase. Somewhat surprisingly, the infrared spectrum of **3-Cr** shows two distinct features at 1540 and 1450 cm^{-1}, which can be assigned to $\nu_{C=O}(dhbq^{2-})$ and $\nu_{C=O}(dhbq^{3-})$, respectively (Figure 4, purple trace). While these features confirm that **3-Cr** displays ligand-based mixed-valence, they also suggest that the mixed-valence states are predominantly localized. The dark purple color of **3-Cr** further supports the presence of localized ligand-valence states, as delocalized mixed-valence materials are typically black. Thus, the formula of **3-Cr** is most accurately written as $(H_2NMe_2)_{1.5}Cr^{III}_2(dhbq^{2-})_{1.5}(dhbq^{3-})_{1.5}$. We note that the extent of ligand reduction in this compound differs from that of the other phases discussed here. The determination of the $dhbq^{2-}$:$dhbq^{3-}$ ratio in **3-Cr** will be discussed below (see Electrochemical Properties section).

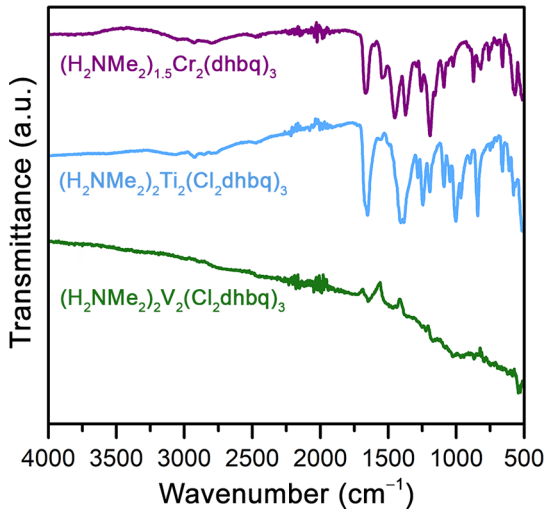

Figure 4. Infrared spectra of **1-Ti**, **2-V**, and **3-Cr**. See Figure S4 for a magnified spectrum of **1-Ti** and **3-Cr** from 2500 to 1000 cm^{-1}.

The electronic structures of **1-Ti** and **2-V** could potentially offer additional complexity, because, unlike iron(III) and chromium(III), titanium(III) and vanadium(III) are strong reductants capable of transferring additional electrons to ligand-based orbitals. Indeed, tris-dioxolene and tris-dithiolene complexes of titanium and vanadium display a wide range of accessible metal oxidation states.[18c,d,23]

In the infrared spectrum of **1-Ti**, no intense peaks are present between 1540 and 1430 cm^{-1}, but a strong, broad feature is centered at 1404 cm^{-1} (Figure 4, blue trace). A carbonyl stretch at such a low frequency would be highly unusual even for Cl_2dhbq^{3-} and is instead more consistent with the presence of ligand mixed-valence in which ligands are present in both the Cl_2dhbq^{3-} and Cl_2dhbq^{4-} states. Based on this, the formula of **1-Ti** is best written as $(H_2NMe_2)_2Ti^{IV}_2(Cl_2dhbq^{3-})_2$-$(Cl_2dhbq^{4-})$ in which four total electrons have been transferred from metal- to ligand-based orbitals. Importantly, the presence of a single broad $\nu_{C=O}$ feature in the infrared spectrum, instead of multiple sharp features, is consistent with increased delocalization in **1-Ti** compared to **3-Cr**. Additionally, while the infrared spectrum of **3-Cr** is flat at higher frequencies, the high frequency end of the **1-Ti** spectrum shows a broad absorbance onset, suggesting the presence of an intervalence charge-transfer (IVCT) band in the near-IR region. A similar absorbance was also observed in the three-dimensional iron phase, and is common for delocalized mixed-valence complexes.[24] This low-energy feature further supports increased valence delocalization in **1-Ti** compared to **3-Cr**.

Interestingly, the infrared spectrum of **2-V** shows a broad absorbance that largely masks the typical vibrational features observed in the mid-IR region (Figure 4, green trace), and only a few weak features are observed. Similar bands have been observed in the mid-IR region of the spectrum for the metallic analogues of $Cu(dcnqi)_2$ (dcnqi = dicyanoquinonediimine), and were assigned to a fully delocalized mixed-valence state.[25] Thus, while we were unable to assign the redox state of the ligand by this technique, the spectrum suggests that the electronic structure of **2-V** is substantially more valence

DOI: 10.1021/jacs.7b13510
J. Am. Chem. Soc. 2018, 140, 3040–3051

delocalized than that of the titanium, chromium, or iron congeners.

UV−Vis−NIR Spectroscopy. Diffuse reflectance UV−vis−NIR spectroscopy was used to further probe the electronic structures of **1-Ti**, **2-V**, and **3-Cr** (Figure 5). Delocalized mixed-valence materials typically display a strong absorbance in the near-infrared region associated with intervalence charge-transfer.[24] This feature was observed near 7000 cm^{-1} in the related two- and three-dimensional iron phases $(NEt_4)_2Fe_2(Cl_2dhbq)_3$ and $(NBu_4)_2Fe_2(dhbq)_3$.[17a,26]

The UV−vis−NIR spectrum of **3-Cr** shows a very weak absorption band in the near-IR region, which we assign to intervalence charge-transfer. Four stronger features are observed at 14 200, 18 900, 24 900, and 29 900 cm^{-1} and are tentatively assigned as a d−d transition enhanced by metal−radical spin-exchange, a ligand-based $\pi-\pi^*$ transition, a charge-transfer transition (ligand-to-metal or metal-to-ligand), and a ligand-based $\pi^*-\pi^*$ transition, respectively. While other assignments for these features are possible, the energies of the transitions align relatively well with those observed in an analogous dinuclear complex, $[Cr_2(tren)_2(Cl_2dhbq)]^{3+}$.[22b] The similarity of the electronic transitions of **3-Cr** to those of a molecular complex and the weak intensity of the IVCT band support the localized electronic structure implied by infrared spectroscopy. Thus, the mixed-valence of **3-Cr** can be assigned as weakly exchanging Robin−Day Class II mixed-valence.[27]

In contrast, the UV−vis−NIR spectrum of **1-Ti** exhibits a continuation of the absorbance onset observed in the mid-IR spectrum that extends across the near-IR region to 12 000 cm^{-1}, with ν_{max} = 5930 cm^{-1}. We assign this feature to an intervalence charge-transfer between ligands in the trianionic and tetraanionic states. Features at higher energies are assigned to ligand-to-metal charge-transfer (17 480 cm^{-1}) and ligand-based transitions (20 790 and 30 860 cm^{-1}). The broad shape of the IVCT band and its similar intensity compared to other charge-transfer transitions in the spectrum suggest that this material lies toward the strongly exchanging end of Robin−Day Class II mixed-valence.[27]

The UV−vis−NIR spectrum of **2-V** differs greatly from those of **1-Ti** and **3-Cr**. The broad absorbance observed in the mid-IR region extends across the near-IR to nearly 12 000 cm^{-1}, and a weaker broad absorbance continues across the visible region. Weak features corresponding to transitions of Cl_2dhbq^{3-} are observed at 21 450 and 29 850 cm^{-1}, confirming that the ligands in **2-V** are at least partially reduced. The broad absorbance in the near-IR region can likely be assigned to the presence of thermally activated charge carriers in **2-V**. Similar absorbance has been observed in doped conductive polymers and mixed-valence molybdenum bronzes.[28] The presence of this feature is indicative of more substantial delocalization between metal and ligand orbitals than is observed in **1-Ti** or **3-Cr**. Consequently, the mixed-valence of **2-V** is best assigned as Robin−Day Class III, although it is not possible with this data to determine whether the delocalized mixed-valence orbitals are predominantly metal-based, ligand-based, or some combination of the two.

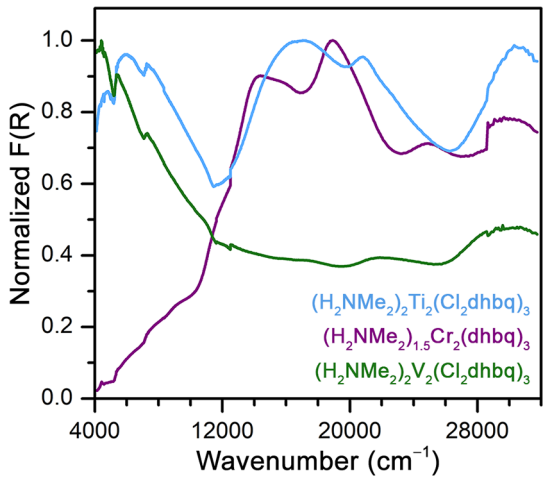

Figure 5. Normalized diffuse reflectance UV−vis−NIR spectra of **1-Ti**, **2-V**, and **3-Cr** shown in blue, green, and purple, respectively. $F(R)$ is the Kubelka−Munk transformation of the raw diffuse reflectance spectrum. $F(R)$ for each material was normalized with the strongest absorbance set to $F(R)$ = 1.

While the mid-IR and UV−vis−NIR spectra do not provide a definitive electronic structure for **2-V**, they are consistent with the presence of significant delocalization and low activation energies for charge transport. As such, it may be inaccurate to describe the distribution of charge in **2-V** by assuming complete metal-to-ligand electron transfer, as would be the case for the nominal formulas $[(V^{III})_2(Cl_2dhbq^{2-})(Cl_2dhbq^{3-})_2]^{2-}$ or $[(V^{III})(V^{IV})(Cl_2dhbq^{3-})_3]^{2-}$, in which two and three electrons, respectively, are transferred from vanadium centers to the ligand scaffold. Indeed, coordination solids displaying partial charge-transfer states—wherein both the metal and ligand have mixed-valence character—can show substantial delocalization or even metallic character.[29] A similar electronic structure for **2-V** may help explain the spectroscopic properties observed here.

Magnetic Properties. Given the presence of paramagnetic metal centers and ligands in **1-Ti**, **2-V**, and **3-Cr**, magnetic susceptibility measurements were used to further probe the electronic structure of these materials. Extended solids containing paramagnetic metals bridged by radical organic ligands have previously been shown to display high-temperature magnetic ordering via antiferromagnetic coupling between metal and ligand spins. Most notable among these systems is $V(tcne)_x$ (tcne = tetracyanoethylene), which orders ferrimagnetically below 400 K.[30] Similarly, the previously discussed two-dimensional iron−chloranilate framework displays ferrimagnetic ordering at 80 K.[13d]

While the absence of metal-based spins in **1-Ti** reduced the likelihood of high-temperature magnetic ordering, dc susceptibility measurements were used to confirm the proposed electronic structure. For the formulation $[Ti^{IV}_2(Cl_2dhbq^{3-})_2(Cl_2dhbq^{4-})]^{2-}$, we expected to observe a room-temperature magnetic moment corresponding to two S = 1/2 spins per formula unit. Instead, the room-temperature $\chi_M T$ value is 0.41 emu·K/mol, which is lower than the expected value of 0.75 emu·K/mol, suggesting the presence of antiferromagnetic interactions between ligand-based spins (Figure 6, top). Upon cooling, $\chi_M T$ decreases monotonically, reaching a value of 0.08 emu·K/mol at 2 K.

A Curie−Weiss fit of the inverse magnetic susceptibility data from 160 to 300 K affords a Curie constant of C = 0.71 emu·K/mol, consistent with the value expected for two ligand-based radicals (Figure 6, bottom). A Curie−Weiss temperature of θ_{CW} = −223 K also supports the presence of relatively strong antiferromagnetic interactions between ligands; however no magnetic ordering is observed even down to 2 K. Given that the ligand-based spins of **1-Ti** are organized into a pseudo-Kagomé lattice (Figure S10), the lack of ordering may be

DOI: 10.1021/jacs.7b13510
J. Am. Chem. Soc. 2018, 140, 3040−3051

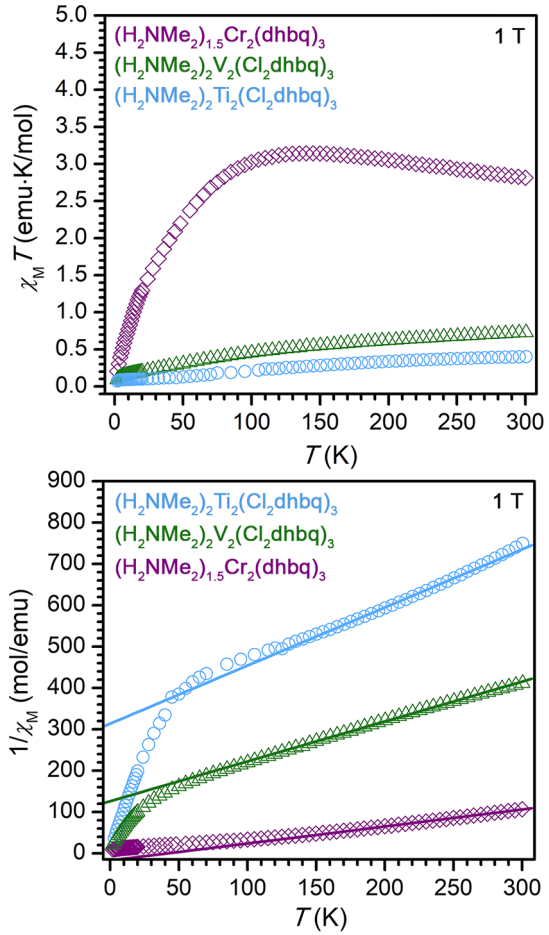

Figure 6. Upper: Dc magnetic susceptibility times temperature versus temperature for **1-Ti** (blue circles), **2-V** (green triangles), and **3-Cr** (purple diamonds). Lower: Inverse magnetic susceptibility versus temperature for **1-Ti**, **2-V**, and **3-Cr**. Curie–Weiss fits to the high temperature data are shown by solid blue, green, and purple lines for **1-Ti**, **2-V**, and **3-Cr**, respectively.

attributed to magnetic frustration. The delocalization of spin-density arising from ligand-based mixed-valence, which distributes radical character across all three ligands in the formula unit, likely enhances this magnetic frustration. The parameter $f = |\theta_{CW}/T_c|$ affords a measure of the frustration in a material, with $f > 10$ suggesting significant frustration.[31] Using 2 K as an upper limit for the ordering temperature, T_c, we find $f >$ 111 for **1-Ti**, indicating that the titanium(IV) centers facilitate strong exchange between paramagnetic ligands that likely leads to the observed frustration.

In contrast to **1-Ti**, compounds **2-V** and **3-Cr** contain both paramagnetic metals and ligands. Such a density of magnetic centers introduces a stronger likelihood for bulk magnetic ordering. In the case of **3-Cr**, the room temperature $\chi_M T$ value of 2.81 emu·K/mol is well below the value of 4.31 emu·K/mol expected for two non-interacting $S = 3/2$ metal-based spins and 1.5 $S = 1/2$ ligand-based spins. With decreasing temperature, $\chi_M T$ initially increases to a peak at 140 K, before sharply decreasing to a value of 0.20 emu·K/mol at 2 K. Notably, the shape of the $\chi_M T$ vs T plot resembles that observed for dinuclear molecular complexes containing two chromium(III) centers bridged by a tetraoxolene radical, although the downturn in the magnetic moment occurs at a much higher temperature.[22b] A Curie–Weiss fit of the inverse susceptibility from 200 to 300 K resulted in $C = 2.43$ emu·K/mol and $\theta_{CW} =$ 42 K. The positive Curie–Weiss temperature suggests weak ferromagnetic interactions are present in the high temperature regime, similar to what was observed in the analogous iron phase. In contrast, fitting the inverse susceptibility from 50 to 2 K afforded a Curie–Weiss temperature of $\theta_{CW} = -37$ K, indicating that antiferromagnetic interactions dominate at lower temperatures.

The lack of magnetic ordering in **3-Cr** can be explained by considering its localized electronic structure. Unlike the iron and titanium congeners, in which spin density is delocalized on all of the ligands, only half of the ligands in **3-Cr** possess sufficient spin density to promote alignment of metal-based spins. At high temperatures (>200 K), strong metal–ligand exchange coupling dominates, leading to small domains of ferrimagnetically coupled chromium-radical units. At temperatures below 140 K, antiferromagnetic interactions between isolated domains of radical-bridged chromium(III) centers dominate the magnetic structure. Thus, while the presence of strong metal–ligand coupling is consistent with the behavior observed in analogous molecular complexes, the localized electronic structure prevents the desired long-range ferrimagnetic ordering.

Given the evidence of a delocalized electronic structure for the vanadium phase from UV–vis–NIR measurements, we expected to observe strong magnetic coupling between the vanadium centers and the radical linkers, which could result in ferrimagnetic or antiferromagnetic ordering, depending on the extent of metal-to-ligand electron transfer. Surprisingly, however, no magnetic ordering is observed in **2-V**, even down to 2 K. Instead, the material displays a room temperature $\chi_M T$ value of 0.73 emu·K/mol that decreases steadily with decreasing temperature to 0.09 emu·K/mol at 2 K. A Curie–Weiss fit to the inverse molar magnetic susceptibility data for **2-V** from 100 to 300 K afforded $C = 1.03$ emu·K/mol and $\theta_{CW} =$ −130 K. The value of the Curie constant suggests a total spin of $S = 1$ per $[V_2(Cl_2dhbq)_3]^{2-}$ formula unit. An $S = 1$ assignment could be made for $[(V^{III})_2(Cl_2dhbq^{2-})(Cl_2dhbq^{3-})_2]^{2-}$ by considering a scenario in which each $S = 1$ vanadium(III) center couples strongly and antiferromagnetically with two $S =$ 1/2 ligand radicals. However, as noted above, such a localized picture of the electronic structure for **2-V** may not be justified. Furthermore, given the similarity of the above formulation to that of the iron congener, it is difficult to rationalize why this formulation would not provoke ferrimagnetic ordering.

One possible explanation for the observed magnetic properties of **2-V** is spin quenching due to the highly covalent nature of its metal–ligand interactions. In vanadium tris-dithiolene complexes, electrons tend to pair in delocalized, low-lying metal–ligand bonding orbitals, yielding overall ligand-centered spins of at most $S = 1/2$.[23c] A similar effect in **2-V** would result in a lower than expected spin density on the ligands, explaining the lack of bulk magnetic order. Such spin quenching in **2-V** would also support the premise that this material has a delocalized electronic structure more accurately described by a band model than by the assignment of formal redox states.

Finally, low-temperature (2 K) magnetization curves were obtained for **1-Ti**, **2-V**, and **3-Cr** (Figure S9); all three materials display closed hysteresis loops.

Electronic Conductivity. The continuous pathways of mixed-valence units in **1-Ti**, **2-V**, and **3-Cr** suggested all three materials may display electronic conductivity. We were

DOI: 10.1021/jacs.7b13510
J. Am. Chem. Soc. 2018, 140, 3040–3051

particularly interested in exploring whether the spectroscopically determined electronic structures would correlate with electronic conductivities. The energy and intensity of the IVCT bands should be related to both the activation barriers to redox hopping and the bulk electronic conductivities.[32] Consequently, the vanadium phase was expected to show the highest conductivity, followed by the titanium and chromium phases. While similar trends linking spectroscopic properties to bulk conductivity have been reported in other materials, there are few examples among metal−organic frameworks.[33]

Room-temperature electronic conductivities of **1-Ti**, **2-V**, and **3-Cr** were measured under an Ar atmosphere using a custom-built two-point screw cell with copper electrodes (Figure S11), and were found to be $2.7(2) \times 10^{-3}$ S/cm, 0.45(3) S/cm, and $1.2(1) \times 10^{-4}$ S/cm, respectively (Figure S12). Thus, the conductivities of these materials follow the expected trend based on the extent of electronic delocalization observed spectroscopically. Notably, while the conductivity of **2-V** is not the highest known for a metal−organic framework, it is surpassed only by materials in which conduction occurs through conjugation at square planar metal sites, and is the highest yet reported for a framework based on oxo-donor linkers.[6b] Given that a pressed pellet measurement is likely to underestimate the intrinsic conductivity of a two-dimensional material, the intrinsic conductivity of **2-V** may actually be several orders of magnitude higher than the value reported here.[7d] The effects of anisotropic charge transport are especially relevant for **2-V** considering that interlayer charge hopping, an important transport pathway in other metal−organic lamellar structures with short interlayer distances, is unlikely to occur due to the interlayer distances of nearly 9 Å.[6d,e,h,34]

To better probe the mechanism of charge transport in these materials, variable-temperature conductivity measurements were performed (Figure 7). Considering the relatively localized electronic structure of **1-Ti** and **3-Cr**, one would expect conductivity to occur via redox-hopping between neighboring ligands in different valence states, rather than through excitation into a delocalized band.[35] Thus, the data for **1-Ti** and **3-Cr** were fit to the polaronic nearest-neighbor hopping model given by eq 1:

$$\sigma T = \sigma_0 \, e^{-E_A/k_B T} \quad (1)$$

These fits yielded activation energies for of 270 and 440 meV, respectively (see also Figure S17). We note that these activation energies are based on a single variable temperature curve. The higher activation energy of **3-Cr** is consistent with its more localized electronic structure and its relatively weak IVCT band.

In contrast, the variable-temperature conductivity of **2-V** could not be fit to the Arrhenius or polaronic models. Indeed, the Arrhenius plot of the variable temperature conductivity data exhibits a distinct curvature indicative of a decreasing activation energy with decreasing temperature (Figure S17). High- and low-temperature linear fits to the Arrhenius plot afforded activation energies of 64 meV at 300 K and 11 meV at 20 K. We note that the low-temperature activation energy is based on a small number of data points and may slightly overestimate the true value. Such behavior is characteristic of a variable-range hopping (VRH) mechanism for charge transport, which is frequently observed in amorphous semiconductors or defect-limited materials displaying Anderson localization.[36] This mechanism has also been observed in organic polymers and coordination solids in which charge transport is limited by electron transport between one-dimensional chains or two-dimensional sheets.[6h,37]

The variable-temperature conductivity of **2-V** was satisfactorily fit with the Efros−Shklovskii variable-range hopping (ES-VRH) model:

$$\sigma = \sigma_0 \, e^{-(T_0/T)^{1/2}} \quad (2)$$

Application of this model afforded a better fit to the data for **2-V** than the three-dimensional Mott VRH model (Figure S17).[38] We note that the observation of field-dependent conductivity below 100 K (Figure S18) is also consistent with the ES-VRH mechanism.[39] The observation of ES variable-range hopping in **2-V** suggests that its conductivity is dominated by localized charge carriers at defect sites, rather than delocalized bands generated by the crystalline material. However, this mechanism of charge transport also implies that the range of intrinsic electronic delocalization in **2-V** is larger than the distance between defect sites, supporting the spectroscopic and magnetic evidence of substantial metal−ligand covalency and long-range electronic communication. Further study is needed to determine whether the trap states inducing variable-range hopping in **2-V** stem from defects at interparticle contacts or from intrinsic defects in the bulk material.

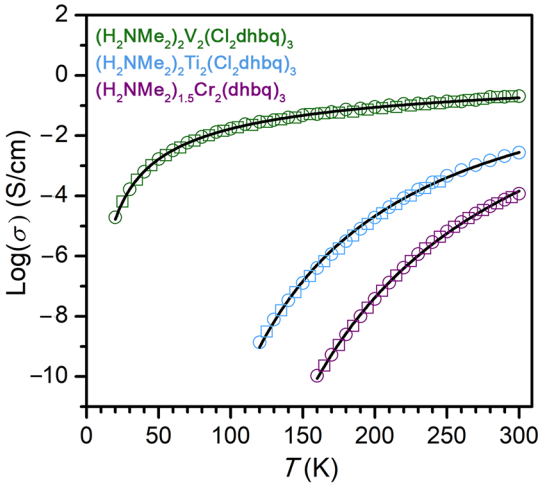

Figure 7. Variable-temperature conductivities of **1-Ti**, **2-V**, and **3-Cr** shown in blue, green, and purple, respectively. Data collected while cooling and warming are represented by circles and squares, respectively. Black lines represent nearest-neighbor hopping fits for **1-Ti** and **3-Cr**, and an Efros−Shklovskii variable-range hopping fit for **2-V**.

Electrochemical Properties. One of the appealing aspects of developing materials combining redox-active metals with redox non-innocent ligands is the potential for tuning their properties post-synthetically by chemical reduction or oxidation. In the previously reported iron semiquinoid materials, post-synthetic reduction afforded frameworks of the type $[Fe^{III}_2(X_2dhbq)_3]^{3-}$, containing iron(III) centers bridged entirely by paramagnetic $dhbq^{3-}$ ligands. This increase in spin density on the ligands led to a substantial increase in the magnetic ordering temperature for both the two- and three-dimensional phases. However, the loss of ligand-based mixed-valence upon reduction lowered both the charge mobility and

DOI: 10.1021/jacs.7b13510
J. Am. Chem. Soc. 2018, 140, 3040−3051

the hole (the majority charge carrier) concentration, resulting in a substantial drop in conductivity.[17]

The possibility of post-synthetic redox tuning in **1-Ti**, **2-V**, and **3-Cr** was investigated through solid-state cyclic voltammetry. By probing electrochemical processes at slow scan rates, bulk electrochemical reactions, rather than just surface-confined reactions, can be monitored.[40] Consequently, integration of the voltammogram can be used to assess the extent of reduction or oxidation. Cyclic voltammograms of **1-Ti**, **2-V**, and **3-Cr** were collected using lithium reference and counter electrodes in a 0.1 M $LiBF_4$ propylene carbonate solution at a scan rate of 30 μV/s (Figure 8). All three materials exhibit quasi-reversible electrochemical oxidative and reductive processes; the half-wave potentials and calculated stoichiometries of reduction and oxidation events are listed in Table S5. Notably, the capacities of **1-Ti** and **3-Cr** are less than three electrons per formula unit, suggesting that ligand-based redox processes are solely responsible for their electrochemical behavior. Ligand-based redox-activity is further supported by comparison to analogous molecular complexes, which require much more reducing potentials to access metal-centered reduction, and in which metal-centered oxidation has not been observed.[15a,18d] In contrast, **2-V** displays a capacity in excess of four electrons per formula unit, suggesting a combination of cationic (metal-based) and anionic (ligand-based) redox activity. Similar behavior has been observed in second- and third-row transition metal oxides, wherein metal−ligand covalency promotes simultaneous cationic and anionic redox activity.[41]

As discussed above, the ligand-based mixed-valence in **3-Cr** arises from partial reduction by the hydrolysis product of DMF. The non-stoichiometric nature of this reductant rendered the $dhbq^{2-}$:$dhbq^{3-}$ ratio in the material ambiguous. As a result, we sought to assess the extent of ligand-based mixed-valency in **3-Cr** electrochemically. To this end, we fabricated two electrochemical cells for separate reduction and oxidation experiments (Figures 8 and S18). Integration of the first oxidative and reductive features of **3-Cr** revealed similar amounts of total charge (Figure S20), and, given the relatively redox-inert nature of Cr(III), we assign these features to ligand-based processes. Thus, integration of the voltammograms supports the previously discussed $dhbq^{2-}$:$dhbq^{3-}$ ratio identified for **3-Cr**, in which half of the ligands are in the trianionic state.

While full characterization of reduced or oxidized analogues of **1-Ti**, **2-V**, and **3-Cr** is beyond the scope of this report, their voltammograms suggest the possibility of isolating materials with improved magnetic performance. Oxidation of **1-Ti** by one electron could give a framework of formula $[Ti^{IV}_2(Cl_2dhbq^{3-})_3]^-$, which would contain d^0 metal centers linked exclusively by radical ligands and could prove useful for studying spin frustration in semiquinoid systems. Similarly, reduction of **2-V** or **3-Cr** could yield materials consisting of trivalent metals bridged by three radical ligands, which might allow the strong local interactions observed here to extend across the lattice to realize a bulk magnetically ordered state. Efforts to isolate and characterize these redox-adjusted materials are underway.

Molecular Orbital Model. Although the electronic conductivities of **1-Ti**, **2-V**, and **3-Cr** are consistent with the electronic structures observed through spectroscopic and magnetic measurements, this data alone does not provide clear design principles for developing new frameworks with improved conductivities and magnetic properties. Given the nature of metal−organic frameworks as fundamentally molecule-based materials, we sought to develop a molecular orbital model to gain insight into the improved conductivity of **2-V** over **1-Ti** and **3-Cr**, as well as the previously reported iron congener. Toward this goal, we first considered the effects of spatial orbital overlap in these systems using the metal−oxygen bond distances as an approximation for spatial overlap. Based on the framework unit cell parameters of these frameworks and the bond distances in related tris-catecholate complexes, we would expect chromium to display the greatest metal−ligand

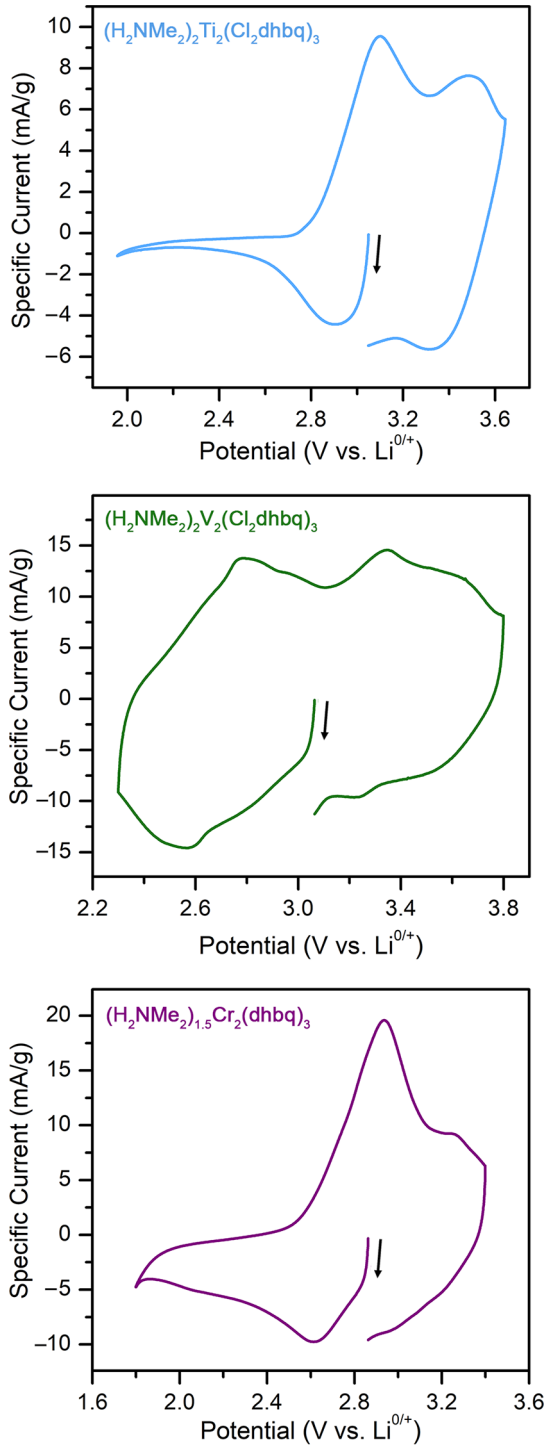

Figure 8. Solid-state cyclic voltammograms of **1-Ti** (top), **2-V** (middle), and **3-Cr** (bottom) collected at 30 μV/s with lithium reference and counter electrodes and 0.1 M $LiBF_4$ electrolyte solution.

DOI: 10.1021/jacs.7b13510
J. Am. Chem. Soc. 2018, 140, 3040−3051

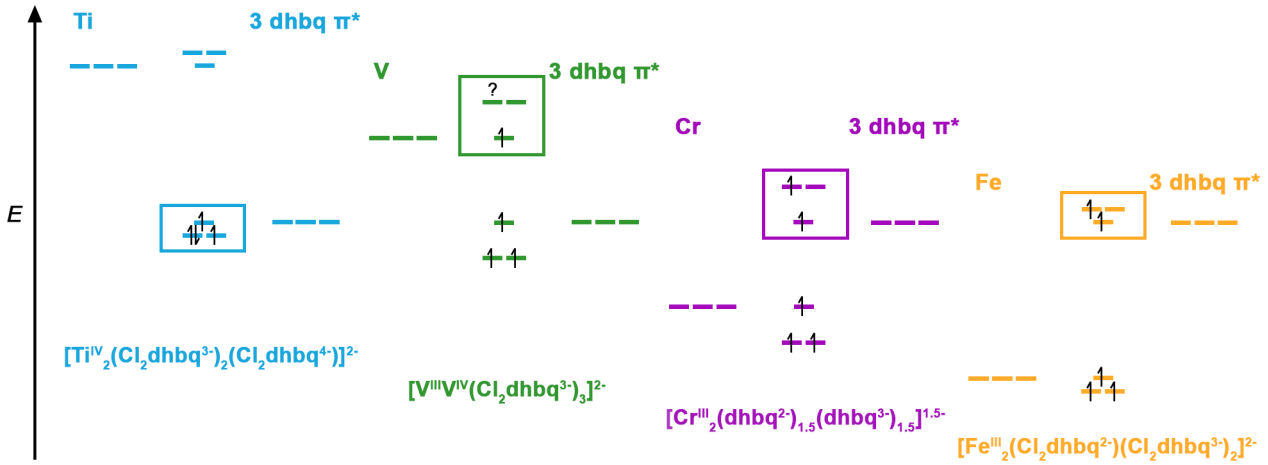

Figure 9. Proposed molecular orbital model of the d–π* interactions in the titanium, vanadium, chromium, and iron semiquinoid phases, assuming a local D_3 symmetry at the metal center. The electrons placed in each orbital are based on the spectroscopically determined redox states of the metals and ligands. The question mark for the vanadium phase indicates the ambiguous formal oxidation state of vanadium in **2-V**. The boxes for each phase indicate the orbitals involved in the intervalence charge-transfer transition. Energy spacings between metal and ligand orbitals are not quantitative, but energies for metal and ligand orbitals are accurate relative to each other.

orbital overlap of the four metals.[18] Additionally, chromium should display more diffuse 3d orbitals than iron, further improving orbital overlap. However, the chromium compound **3-Cr** was observed to have the most localized electronic structure, suggesting that spatial overlap does not provide an adequate explanation for the trends observed for these materials.

Alternatively, we sought to rationalize the observed properties using an orbital energy alignment argument. Indeed, orbital interaction diagrams for the octahedral building units in these frameworks should be analogous to those of structurally similar tris-catecholate complexes (Figure S21). A qualitative interaction diagram of the π orbitals in **1-Ti**, **2-V**, **3-Cr**, and the iron congener is shown in Figure 9. For simplicity, all ligand orbitals are shown at equal energies, as only a small difference is expected for dhbq^{n-} and Cl$_2$dhbq^{n-} (see Supporting Information for more details). Although this orbital model substantially simplifies the metal–ligand interactions in these systems, it provides insight into the effects of orbital energy alignment on electronic structure and conductivity. We note that, because the metal to ligand ratio in these diagrams (1:3) differs from that in the actual material (2:3), the illustrated electron counts are based on the spectroscopically determined redox states of the metals and ligands.

For iron and chromium, the 3d orbitals are lower in energy than the π* orbitals of the ligand, but the 3d–π* energy spacing should be smaller for chromium than for iron. While this arrangement would be expected to result in a stronger metal–ligand exchange coupling, it also leads to a larger energy separation between the nonbonding and antibonding ligand-centered orbitals. In these materials, this energy spacing defines the energy of intervalence charge-transfer, which should be closely related to the barrier to charge transport.[33,42] The increase in the energy of the IVCT transition for chromium relative to iron matches our spectroscopic observations and may explain the increased electronic localization in the chromium phase.

Based on the observation of additional ligand reduction in **1-Ti**, and the strong likelihood that a similar level of ligand reduction occurs in **2-V**, the 3d orbitals of titanium and vanadium must lie higher in energy than the π* orbitals of the ligands. The extent of ligand reduction in **1-Ti** suggests that the 3d orbitals must lie sufficiently high that reduction of the ligand to the tetraanionic state is favored. This arrangement in turn requires a large 3d–π* energy difference, resulting in a small energy separation between the bonding and nonbonding ligand-based orbitals. Satisfyingly, the low-energy IVCT feature predicted by this orbital model is in agreement with the spectroscopic data and the activation energy obtained in variable-temperature conductivity measurements of **1-Ti**.

It is important to note that the molecular orbital model presented here is not sufficiently complex to explain the electronic structure of **2-V**, since a mononuclear model cannot accurately depict any metal-based mixed-valence, nor can it account for the possibility of a partial charge-transfer state. Furthermore, we have not accounted for any spin quenching, although the magnetic susceptibility data suggests that some electron pairing must occur in the low-lying metal–ligand bonding orbitals. As such, the energy of the intervalence charge-transfer in this system is not accurately represented by the highlighted transition in this model.

While our orbital model fails to completely describe the electronic structure of **2-V**, it does suggest that the 3d orbitals of vanadium may lie at an appropriate energy to form highly covalent and delocalized molecular orbitals with the ligand. Such interactions are supported by the strong absorption observed in the near-infrared spectrum of the compound, in addition to its enhanced electrochemical capacity.[43] As a result, band structure calculations may be required to provide a more accurate depiction of the metal–ligand interactions in **2-V**. Despite these limitations, this orbital model of **2-V** supports the oft-cited prediction that increased covalency between metal and ligand orbitals can facilitate highly delocalized electronic structures.[44] Indeed, metal–ligand covalency has previously been used to explain the room temperature magnetic ordering of V(tcne)$_x$ as well as the metallic character of Cu(Me$_2$-DCNQI)$_2$.[45] Research on charge-transfer complexes has demonstrated that control of donor–acceptor energy alignment resulting in partial charge transfer can lead to exceptionally high conductivities.[46] While other reports have made note of energy tuning as an appealing strategy for improving the conductivity of metal–organic frameworks, these semiquinoid frameworks

DOI: 10.1021/jacs.7b13510
J. Am. Chem. Soc. 2018, 140, 3040–3051

are among the few metal−organic materials that demonstrate this trend.[8]

These molecular orbital models also suggest that energy alignment, on its own, may not be sufficient to improve the conductivities of metal−organic materials. In fact, the localization in the chromium phase may be related to its improved energy alignment compared to the iron phase, which results in a higher energy IVCT transition. Consequently, the development of metal−organic frameworks displaying delocalized electronic structures will require control over the energies of charge-transfer transitions associated with charge transport.

Of course, these models substantially simplify the orbital interactions present in a true material. However, they do suggest it may be possible to predict optimal metal−ligand pairings for particular coordination geometries, promoting the design of new conductive frameworks based on the established principles of coordination chemistry. Specifically, comparisons of metal redox couples to ligand reduction potentials across a wide-range of materials may provide a more quantitative method for identifying new synthetic targets.

CONCLUSIONS

The foregoing results provide a rare assessment of the variations in electronic conductivity across an isostructural series of metal−organic frameworks, as measured for new two-dimensional semiquinoid-linked frameworks based on titanium, vanadium, and chromium. Using spectroscopic and magnetic susceptibility data, we identified a diverse range of electronic structures across the three materials. The vanadium phase was shown to display substantial electronic delocalization, consistent with the presence of significant metal−ligand covalency. The electronic structures were further shown to correlate with bulk conductivities, and an orbital model was established suggesting that the energy alignment of metal 3d and ligand π^* orbitals dictates the extent of delocalization in these frameworks. It is expected that a similar orbital treatment could be extended to other frameworks containing redox non-innocent ligands.

The results further suggest potential challenges confronting the design of new materials with redox-active ligands intended to simultaneously exhibit a high conductivity and a high magnetic ordering temperature. Specifically, while it may be desirable to access very covalent metal−ligand interactions for enhancing electronic conductivity, this covalency may also result in the quenching of ligand-based spins, precluding the possibility of ferrimagnetic ordering. Consequently, enhanced conductivity and magnetic ordering may be at odds in this class of materials.

Efforts to study the nature of reduction and oxidation in **1-Ti**, **2-V**, and **3-Cr**, as well as the bulk properties of the redox-adjusted materials, are underway. Seebeck coefficient and field effect transistor measurements could additionally provide information about the nature of the charge carriers in these materials. The synthesis of analogous materials based upon second- and third-row transition metals may also be valuable for further refinement of the orbital model discussed here. Finally, the combination of experimental and computational methods will undoubtedly prove important in further understanding the role of covalency in these materials and identifying synthetic targets for new electronically active materials.

ASSOCIATED CONTENT

Supporting Information

The Supporting Information is available free of charge on the ACS Publications website at DOI: 10.1021/jacs.7b13510.

Additional experimental procedures, powder X-ray diffraction data, infrared spectroscopy, variable-temperature magnetism, variable-temperature conductivity, and electrochemical data (PDF)

AUTHOR INFORMATION

Corresponding Author

*jrlong@berkeley.edu

ORCID

Jeffrey R. Long: 0000-0002-5324-1321

Notes

The authors declare no competing financial interest.

ACKNOWLEDGMENTS

This research was supported by National Science Foundation (NSF) Award No. DMR-1611525, with the exception of the measurement and analysis of the magnetic susceptibility data, which were supported by the Nanoporous Materials Genome Center of the U.S. Department of Energy, Office of Basic Energy Sciences, Division of Chemical Sciences, Geosciences and Biosciences under Award No. DE-FG02-17ER16362. Powder X-ray diffraction data were collected on beamlines 11-BM and 17-BM at the Advanced Photon Source at Argonne National Laboratory, which is supported by the U.S. Department of Energy, Office of Science, Office of Basic Energy Sciences, under Contract No. DE-AC02-06CH11357. Data from beamline 11-BM were collected as part of the 2017 Modern Methods in Rietveld Refinement and Structural Analysis School with support from its sponsors. We further thank the NSF for graduate fellowship support of L.E.D.; Julia Oktawiec, Henry Jiang, Saul Lapidus, and the 17-BM staff for assisting with the powder X-ray diffraction experiments; Dr. Mike Aubrey and Dr. Valentina Colombo for helpful conversations and experimental assistance; and Dr. K. R. Meihaus for editorial assistance.

REFERENCES

(1) (a) Long, J. R.; Yaghi, O. M. *Chem. Soc. Rev.* **2009**, *38*, 1213. (b) Zhou, H. C.; Kitagawa, S. *Chem. Soc. Rev.* **2014**, *43*, 5415.

(2) Li, B.; Wen, H. M.; Cui, Y.; Zhou, W.; Qian, G.; Chen, B. *Adv. Mater.* **2016**, *28*, 8819.

(3) Hendon, C. H.; Tiana, D.; Walsh, A. *Phys. Chem. Chem. Phys.* **2012**, *14*, 13120.

(4) (a) Ferey, G.; Millange, F.; Morcrette, M.; Serre, C.; Doublet, M. L.; Greneche, J. M.; Tarascon, J. M. *Angew. Chem., Int. Ed.* **2007**, *46*, 3259. (b) Dechambenoit, P.; Long, J. R. *Chem. Soc. Rev.* **2011**, *40*, 3249. (c) Erickson, K. J.; Leonard, F.; Stavila, V.; Foster, M. E.; Spataru, C. D.; Jones, R. E.; Foley, B. M.; Hopkins, P. E.; Allendorf, M. D.; Talin, A. A. *Adv. Mater.* **2015**, *27*, 3453. (d) Campbell, M. G.; Sheberla, D.; Liu, S. F.; Swager, T. M.; Dinca, M. *Angew. Chem., Int. Ed.* **2015**, *54*, 4349. (e) Campbell, M. G.; Liu, S. F.; Swager, T. M.; Dinca, M. *J. Am. Chem. Soc.* **2015**, *137*, 13780.

(5) Sun, L.; Campbell, M. G.; Dinca, M. *Angew. Chem., Int. Ed.* **2016**, *55*, 3566.

(6) (a) Narayan, T. C.; Miyakai, T.; Seki, S.; Dincă, M. *J. Am. Chem. Soc.* **2012**, *134*, 12932. (b) Hmadeh, M.; Lu, Z.; Liu, Z.; Gándara, F.; Furukawa, H.; Wan, S.; Augustyn, V.; Chang, R.; Liao, L.; Zhou, F.; Perre, E.; Ozolins, V.; Suenaga, K.; Duan, X.; Dunn, B.; Yamamto, Y.; Terasaki, O.; Yaghi, O. M. *Chem. Mater.* **2012**, *24*, 3511. (c) Sun, L.;

DOI: 10.1021/jacs.7b13510
J. Am. Chem. Soc. 2018, 140, 3040−3051

Miyakai, T.; Seki, S.; Dinca, M. *J. Am. Chem. Soc.* **2013**, *135*, 8185. (d) Kambe, T.; Sakamoto, R.; Hoshiko, K.; Takada, K.; Miyachi, M.; Ryu, J. H.; Sasaki, S.; Kim, J.; Nakazato, K.; Takata, M.; Nishihara, H. *J. Am. Chem. Soc.* **2013**, *135*, 2462. (e) Sheberla, D.; Sun, L.; Blood-Forsythe, M. A.; Er, S.; Wade, C. R.; Brozek, C. K.; Aspuru-Guzik, A.; Dinca, M. *J. Am. Chem. Soc.* **2014**, *136*, 8859. (f) Talin, A. A.; Centrone, A.; Ford, A. C.; Foster, M. E.; Stavila, V.; Haney, P.; Kinney, R. A.; Szalai, V.; El Gabaly, F.; Yoon, H. P.; Leonard, F.; Allendorf, M. D. *Science* **2014**, *343*, 66. (g) Sun, L.; Hendon, C. H.; Minier, M. A.; Walsh, A.; Dinca, M. *J. Am. Chem. Soc.* **2015**, *137*, 6164. (h) Huang, X.; Sheng, P.; Tu, Z.; Zhang, F.; Wang, J.; Geng, H.; Zou, Y.; Di, C. A.; Yi, Y.; Sun, Y.; Xu, W.; Zhu, D. *Nat. Commun.* **2015**, *6*, 7408. (i) Chen, D.; Xing, H.; Su, Z.; Wang, C. *Chem. Commun.* **2016**, *52*, 2019.

(7) (a) Takaishi, S.; Hosoda, M.; Kajiwara, T.; Miyasaka, H.; Yamashita, M.; Nakanishi, Y.; Kitagawa, Y.; Yamaguchi, K.; Kobayashi, A.; Kitagawa, H. *Inorg. Chem.* **2009**, *48*, 9048. (b) Kobayashi, Y.; Jacobs, B.; Allendorf, M. D.; Long, J. R. *Chem. Mater.* **2010**, *22*, 4120. (c) Gandara, F.; Uribe-Romo, F. J.; Britt, D. K.; Furukawa, H.; Lei, L.; Cheng, R.; Duan, X.; O'Keeffe, M.; Yaghi, O. M. *Chem. - Eur. J.* **2012**, *18*, 10595. (d) Kambe, T.; Sakamoto, R.; Kusamoto, T.; Pal, T.; Fukui, N.; Hoshiko, K.; Shimojima, T.; Wang, Z.; Hirahara, T.; Ishizaka, K.; Hasegawa, S.; Liu, F.; Nishihara, H. *J. Am. Chem. Soc.* **2014**, *136*, 14357. (e) Aubrey, M. L.; Long, J. R. *J. Am. Chem. Soc.* **2015**, *137*, 13594.

(8) Sun, L.; Hendon, C. H.; Park, S. S.; Tulchinsky, Y.; Wan, R.; Wang, F.; Walsh, A.; Dincă, M. *Chem. Sci.* **2017**, *8*, 4450.

(9) Park, S. S.; Hontz, E. R.; Sun, L.; Hendon, C. H.; Walsh, A.; Van Voorhis, T.; Dinca, M. *J. Am. Chem. Soc.* **2015**, *137*, 1774.

(10) (a) Potember, R. S.; Poehler, T. O.; Cowan, D. O. *Appl. Phys. Lett.* **1979**, *34*, 405. (b) Clérac, R.; O'Kane, S.; Cowen, J.; Ouyang, X.; Heintz, R.; Zhao, H.; Bazile, M. J.; Dunbar, K. R. *Chem. Mater.* **2003**, *15*, 1840.

(11) (a) Pierpont, C. G.; Buchanan, R. M. *Coord. Chem. Rev.* **1981**, *38*, 45. (b) Eisenberg, R.; Gray, H. B. *Inorg. Chem.* **2011**, *50*, 9741.

(12) (a) Aquino, M. A.; Lee, F. L.; Gabe, E. J.; Bensimon, C.; Greedan, J. E.; Crutchley, R. J. *J. Am. Chem. Soc.* **1992**, *114*, 5130. (b) Brunschwig, B. S.; Creutz, C.; Sutin, N. *Chem. Soc. Rev.* **2002**, *31*, 168.

(13) (a) Dei, A.; Gatteschi, D.; Pardi, L.; Russo, U. *Inorg. Chem.* **1991**, *30*, 2589. (b) Gupta, P.; Das, A.; Basuli, F.; Castineiras, A.; Sheldrick, W. S.; Mayer-Figge, H.; Bhattacharya, S. *Inorg. Chem.* **2005**, *44*, 2081. (c) Nakabayashi, K.; Ohkoshi, S. *Inorg. Chem.* **2009**, *48*, 8647. (d) Jeon, I.-R.; Negru, B.; Van Duyne, R. P.; Harris, T. D. *J. Am. Chem. Soc.* **2015**, *137*, 15699.

(14) Min, K. S.; DiPasquale, A. G.; Golen, J. A.; Rheingold, A. L.; Miller, J. S. *J. Am. Chem. Soc.* **2007**, *129*, 2360.

(15) (a) Downs, H. H.; Buchanan, R. M.; Pierpont, C. G. *Inorg. Chem.* **1979**, *18*, 1736. (b) Gordon, D. J.; Fenske, R. F. *Inorg. Chem.* **1982**, *21*, 2907.

(16) (a) Weiss, A.; Riegler, E.; Robl, C. *Z. Naturforsch., B: J. Chem. Sci.* **1986**, *41*, 1501. (b) Luo, T.-T.; Liu, Y.-H.; Tsai, H.-L.; Su, C.-C.; Ueng, C.-H.; Lu, K.-L. *Eur. J. Inorg. Chem.* **2004**, *2004*, 4253. (c) Abrahams, B. F.; Hudson, T. A.; McCormick, L. J.; Robson, R. *Cryst. Growth Des.* **2011**, *11*, 2717. (d) Atzori, M.; Benmansour, S.; Minguez Espallargas, G.; Clemente-Leon, M.; Abherve, A.; Gomez-Claramunt, P.; Coronado, E.; Artizzu, F.; Sessini, E.; Deplano, P.; Serpe, A.; Mercuri, M. L.; Gomez Garcia, C. J. *Inorg. Chem.* **2013**, *52*, 10031.

(17) (a) Darago, L. E.; Aubrey, M. L.; Yu, C. J.; Gonzalez, M. I.; Long, J. R. *J. Am. Chem. Soc.* **2015**, *137*, 15703. (b) DeGayner, J. A.; Jeon, I. R.; Sun, L.; Dinca, M.; Harris, T. D. *J. Am. Chem. Soc.* **2017**, *139*, 4175.

(18) (a) Rosenheim, A.; Sorge, O. *Ber. Dtsch. Chem. Ges. B* **1920**, *53*, 932. (b) Isied, S. S.; Kuo, G.; Raymond, K. N. *J. Am. Chem. Soc.* **1976**, *98*, 1763. (c) Cooper, S. R.; Koh, Y. B.; Raymond, K. N. *J. Am. Chem. Soc.* **1982**, *104*, 5092. (d) Borgias, B. A.; Cooper, S. R.; Koh, Y. B.; Raymond, K. N. *Inorg. Chem.* **1984**, *23*, 1009.

(19) An amorphous material generated from the reaction of $V(CO)_6$ and H_2dhbq has previously been reported: Thorum, M. S.; Taliaferro, M. L.; Min, K. S.; Miller, J. S. *Polyhedron* **2007**, *26*, 2247.

(20) Halis, S.; Inge, A. K.; Dehning, N.; Weyrich, T.; Reinsch, H.; Stock, N. *Inorg. Chem.* **2016**, *55*, 7425.

(21) Murase, R.; Abrahams, B. F.; D'Alessandro, D. M.; Davies, C. G.; Hudson, T. A.; Jameson, G. N. L.; Moubaraki, B.; Murray, K. S.; Robson, R.; Sutton, A. L. *Inorg. Chem.* **2017**, *56*, 9025.

(22) (a) Min, K. S.; Rheingold, A. L.; Dipasquale, A.; Miller, J. S. *Inorg. Chem.* **2006**, *45*, 6135. (b) Guo, D.; McCusker, J. K. *Inorg. Chem.* **2007**, *46*, 3257.

(23) (a) Könemann, M.; Stüer, W.; Kirschbaum, K.; Giolando, D. M. *Polyhedron* **1994**, *13*, 1415. (b) Morris, A. M.; Pierpont, C. G.; Finke, R. G. *Inorg. Chem.* **2009**, *48*, 3496. (c) Sproules, S.; Weyhermuller, T.; Debeer, S.; Wieghardt, K. *Inorg. Chem.* **2010**, *49*, 5241.

(24) Torrance, J. B.; Scott, B. A.; Welber, B.; Kaufman, F. B.; Seiden, P. E. *Phys. Rev. B: Condens. Matter Mater. Phys.* **1979**, *19*, 730.

(25) Yamakita, Y.; Furukawa, Y.; Kobayashi, A.; Tasumi, M.; Kato, R.; Kobayashi, H. *J. Chem. Phys.* **1994**, *100*, 2449.

(26) Kingsbury, C. J.; Abrahams, B. F.; D'Alessandro, D. M.; Hudson, T. A.; Murase, R.; Robson, R.; White, K. F. *Cryst. Growth Des.* **2017**, *17*, 1465.

(27) Robin, M. B.; Day, P. *Adv. Inorg. Chem. Radiochem.* **1968**, *10*, 247.

(28) (a) Dickens, P. G.; Neild, D. J. *Trans. Faraday Soc.* **1968**, *64*, 13. (b) Chung, T. C.; Kaufman, J. H.; Heeger, A. J.; Wudl, F. *Phys. Rev. B: Condens. Matter Mater. Phys.* **1984**, *30*, 702.

(29) Kobayashi, A.; Kato, R.; Kobayashi, H.; Mori, T.; Inokuchi, H. *Solid State Commun.* **1987**, *64*, 45.

(30) Manriquez, J. M.; Yee, G. T.; McLean, R. S.; Epstein, A. J.; Miller, J. S. *Science* **1991**, *252*, 1415.

(31) Balents, L. *Nature* **2010**, *464*, 199.

(32) (a) England, S. J.; Kathirgamanathan, P.; Rosseinsky, D. R. *J. Chem. Soc., Chem. Commun.* **1980**, 840. (b) Bredas, J. L.; Calbert, J. P.; da Silva Filho, D. A.; Cornil, J. *Proc. Natl. Acad. Sci. U. S. A.* **2002**, *99*, 5804. (c) D'Alessandro, D. M.; Keene, F. R. *Chem. Rev.* **2006**, *106*, 2270.

(33) Collman, J. P.; McDevitt, J. T.; Yee, G. T.; Zisk, M. B.; Torrance, J. B.; Little, W. A. *Synth. Met.* **1986**, *15*, 129.

(34) Clough, A. J.; Skelton, J. M.; Downes, C. A.; de la Rosa, A. A.; Yoo, J. W.; Walsh, A.; Melot, B. C.; Marinescu, S. C. *J. Am. Chem. Soc.* **2017**, *139*, 10863.

(35) Schmidt, R.; Basu, A.; Brinkman, A. W. *Phys. Rev. B: Condens. Matter Mater. Phys.* **2005**, *72*, 115101.

(36) Mott, N. F. *Philos. Mag.* **1969**, *19*, 835.

(37) Kivelson, S. *Phys. Rev. Lett.* **1981**, *46*, 1344.

(38) Shklovskii, B. I.; Efros, A. L. *Electronic Properties of Doped Semiconductors*; Springer-Verlag: New York, 1984.

(39) (a) Stallinga, P. *Adv. Mater.* **2011**, *23*, 3356. (b) Joung, D.; Khondaker, S. I. *Phys. Rev. B: Condens. Matter Mater. Phys.* **2012**, *86*, 235423.

(40) (a) Yu, D. Y. W.; Fietzek, C.; Weydanz, W.; Donoue, K.; Inoue, T.; Kurokawa, H.; Fujitani, S. *J. Electrochem. Soc.* **2007**, *154*, A253. (b) Zhu, Y.; Gao, T.; Fan, X.; Han, F.; Wang, C. *Acc. Chem. Res.* **2017**, *50*, 1022.

(41) (a) Sathiya, M.; Rousse, G.; Ramesha, K.; Laisa, C. P.; Vezin, H.; Sougrati, M. T.; Doublet, M. L.; Foix, D.; Gonbeau, D.; Walker, W.; Prakash, A. S.; Ben Hassine, M.; Dupont, L.; Tarascon, J. M. *Nat. Mater.* **2013**, *12*, 827. (b) Pearce, P. E.; Perez, A. J.; Rousse, G.; Saubanere, M.; Batuk, D.; Foix, D.; McCalla, E.; Abakumov, A. M.; Van Tendeloo, G.; Doublet, M. L.; Tarascon, J. M. *Nat. Mater.* **2017**, *16*, 580.

(42) Atanasov, M.; Barras, J. L.; Benco, L.; Daul, C. *J. Am. Chem. Soc.* **2000**, *122*, 4718.

(43) Chirik, P. J. *Inorg. Chem.* **2011**, *50*, 9737.

(44) Leong, C. F.; Usov, P. M.; D'Alessandro, D. M. *MRS Bull.* **2016**, *41*, 858.

DOI: 10.1021/jacs.7b13510
J. Am. Chem. Soc. 2018, 140, 3040−3051

(45) (a) Mori, T.; Inokuchi, H.; Kobayashi, A.; Kato, R.; Kobayashi, H. *Phys. Rev. B: Condens. Matter Mater. Phys.* **1988**, *38*, 5913. (b) Miller, J. S. *Polyhedron* **2009**, *28*, 1596.
(46) Torrance, J. B.; Vazquez, J. E.; Mayerle, J. J.; Lee, V. Y. *Phys. Rev. Lett.* **1981**, *46*, 253.

DOI: 10.1021/jacs.7b13510
J. Am. Chem. Soc. 2018, 140, 3040−3051